FLEA: Fresnel-limited extraction algorithm applied to spectral phase interferometry for direct field reconstruction (SPIDER)

Alessia Pasquazi,[1,*] Marco Peccianti,[2] José Azaña,[1] David J. Moss,[3] and Roberto Morandotti[1]

[1]*INRS Énergie, Matériaux et Télécommunications, 1650 Blvd. Lionel Boulet, Varennes (Québec), J3X 1S2, Canada*
[2]*Institute for Complex Systems - CNR, UOS Montelibretti, Via dei Taurini 19, 00185 Rome, Italy*
[3]*Centre for Ultra-high Bandwidth Devices for Optical Systems (CUDOS),and the Institute of Photonics and Optical Science (IPOS), School of Physics, University of Sydney, Sydney, NSW 2006, Australia*
[*]*alessia.pasquazi@gmail.com*

Abstract: We present an extraction algorithm for spectral phase interferometry for direct field reconstruction (SPIDER) in the so-called X-SPIDER configuration. Our approach largely extends the measurable time windows of pulses without requiring any modification to the experimental X-SPIDER setup.

©2013 Optical Society of America

OCIS codes: (120.5050) Phase measurement; (190.4223) Nonlinear wave mixing.

References and links

1. I. A. Walmsley and C. Dorrer, "Characterization of ultrashort electromagnetic pulses," Adv. Opt. Photonics **1**(2), 308–437 (2009).
2. R. Slavík, F. Parmigiani, J. Kakande, C. Lundström, M. Sjödin, P. A. Andrekson, R. Weerasuriya, S. Sygletos, A. D. Ellis, L. Grüner-Nielsen, D. Jakobsen, S. Herstrøm, R. Phelan, J. O'Gorman, A. Bogris, D. Syvridis, S. Dasgupta, P. Petropoulos, and D. J. Richardson, "All-optical phase and amplitude regenerator for next-generation telecommunications systems," Nat. Photonics **4**(10), 690–695 (2010).
3. R.-J. Essiambre, G. Kramer, P. J. Winzer, G. J. Foschini, and B. Goebel, "Capacity limits of optical fiber networks," J. Lightwave Technol. **28**(4), 662–701 (2010).
4. N. K. Fontaine, R. Scott, L. Zhou, F. M. Soares, J. Heritage, and S. Yoo, "Real-time full-field arbitrary optical waveform measurement," Nat. Photonics **4**(4), 248–254 (2010).
5. Z. Jiang, C.-B. Huang, D. E. Leaird, and A. Weiner, "Optical arbitrary waveform processing of more than 100 spectral comb lines," Nat. Photonics **1**(8), 463–467 (2007).
6. S. T. Cundiff and A. M. Weiner, "Optical arbitrary waveform generation," Nat. Photonics **4**(11), 760–766 (2010).
7. M. A. Foster, R. Salem, D. F. Geraghty, A. C. Turner-Foster, M. Lipson, and A. L. Gaeta, "Silicon-chip-based ultrafast optical oscilloscope," Nature **456**(7218), 81–84 (2008).
8. R. Salem, M. A. Foster, A. C. Turner, D. F. Geraghty, M. Lipson, and A. L. Gaeta, "Optical time lens based on four-wave mixing on a silicon chip," Opt. Lett. **33**(10), 1047–1049 (2008).
9. A. Pasquazi, Y. Park, S. T. Chu, B. E. Little, F. Légaré, R. Morandotti, J. Azaña, and D. J. Moss, "Time-lens measurement of subpicosecond optical pulses in CMOS compatible high-index glass waveguides," IEEE J. Sel. Top. Quantum Electron. **18**(2), 629–636 (2012).
10. E. K. Tien, X. Z. Sang, F. Qing, Q. Song, and O. Boyraz, "Ultrafast pulse characterization using cross phase modulation in silicon," Appl. Phys. Lett. **95**(5), 051101 (2009).
11. C. V. Bennett, R. P. Scott, and B. H. Kolner, "Temporal magnification and reversal of 100 Gb/s optical-data with an up-conversion time microscope," Appl. Phys. Lett. **65**(20), 2513–2515 (1994).
12. R. Trebino, "Frequency resolved optical gating: the measurement of ultrashort optical pulses," (Kluwer Academic, 2002).
13. C. Iaconis and I. A. Walmsley, "Spectral phase interferometry for direct electric-field reconstruction of ultrashort optical pulses," Opt. Lett. **23**(10), 792–794 (1998).
14. C. Iaconis and I. A. Walmsley, "Self-referencing spectral interferometry for measuring ultrashort optical pulses," IEEE J. Quantum Electron. **35**(4), 501–509 (1999).
15. M. Takeda, H. Ina, and S. Kobayashi, "Fourier-transform method of fringe-pattern analysis for computer-based topography and interferometry," J. Opt. Soc. Am. **72**(1), 156–160 (1982).
16. M. Hirasawa, N. Nakagawa, K. Yamamoto, R. Morita, H. Shigekawa, and M. Yamashita, "Sensitivity improvement of spectral phase interferometry for direct electric-field reconstruction for the characterization of low-intensity femtosecond pulses," Appl. Phys. B **74**(9 Suppl. S), s225–s229 (2002).

17. P. Londero, M. E. Anderson, C. Radzewicz, C. Iaconis, and I. A. Walmsley, "Measuring ultrafast pulses in the near-ultraviolet using spectral phase interferometry for direct electric field reconstruction," J. Mod. Opt. **50**, 179–184 (2003).
18. L. Gallmann, D. H. Sutter, N. Matuschek, G. Steinmeyer, U. Keller, C. Iaconis, and I. A. Walmsley, "Characterization of sub-6-fs optical pulses with spectral phase interferometry for direct electric-field reconstruction," Opt. Lett. **24**(18), 1314–1316 (1999).
19. C. Dorrer, B. de Beauvoir, C. Le Blanc, S. Ranc, J.-P. Rousseau, P. Rousseau, J.-P. Chambaret, and F. Salin, "Single-shot real-time characterization of chirped-pulse amplification systems by spectral phase interferometry for direct electric-field reconstruction," Opt. Lett. **24**(22), 1644–1646 (1999).
20. J. Wemans, G. Figueira, N. Lopes, and L. Cardoso, "Self-referencing spectral phase interferometry for direct electric-field reconstruction with chirped pulses," Opt. Lett. **31**(14), 2217–2219 (2006).
21. A. Pasquazi, M. Peccianti, Y. Park, B. E. Little, S. T. Chu, R. Morandotti, J. Azaña, and D. J. Moss, "Sub-picosecond phase-sensitive optical pulse characterization on a chip," Nat. Photonics **5**(10), 618–623 (2011).
22. J. Bromage, C. Dorrer, I. A. Begishev, N. G. Usechak, and J. D. Zuegel, "Highly sensitive, single-shot characterization for pulse widths from 0.4 to 85 ps using electro-optic shearing interferometry," Opt. Lett. **31**(23), 3523–3525 (2006).
23. D. R. Austin, T. Witting, and I. A. Walmsley, "High precision self-referenced phase retrieval of complex pulses with multiple-shearing spectral interferometry," J. Opt. Soc. Am. B **26**(9), 1818–1830 (2009).
24. T. Witting, D. R. Austin, and I. A. Walmsley, "Ultrashort pulse characterization by spectral shearing interferometry with spatially chirped ancillae," Opt. Express **17**(21), 18983–18994 (2009).
25. D. R. Austin, T. Witting, and I. A. Walmsley, "Resolution of the relative phase ambiguity in spectral shearing interferometry of ultrashort pulses," Opt. Lett. **35**(12), 1971–1973 (2010).
26. J. Cohen, P. Bowlan, V. Chauhan, P. Vaughan, and R. Trebino, "Single-shot multiple-delay crossed-beam spectral interferometry for measuring extremely complex pulses," Opt. Commun. **284**(15), 3785–3794 (2011).
27. L. Cohen, "Wigner distribution for finite duration or band-limited signals and limiting cases," IEEE Trans. Acoust. Speech **35**(6), 796–806 (1987).
28. F. Hlawatsch, "Interference terms in the Wigner distribution," Digit. Signal Process. **84**, 363–367 (1984).
29. C. Dorrer and I. A. Walmsley, "Precision and consistency criteria in spectral phase interferometry for direct electric-field reconstruction," J. Opt. Soc. Am. B **19**(5), 1030–1038 (2002).
30. C. Dorrer and I. A. Walmsley, "Accuracy criterion for ultrashort pulse characterization techniques: application to spectral phase interferometry for direct electric field reconstruction," J. Opt. Soc. Am. B **19**(5), 1019–1029 (2002).

1. Introduction

Phase-sensitive measurement techniques [1] for the characterization of ultrafast (< 1ps) optical pulses with large spectral bandwidths and long temporal windows (>100ps) are becoming increasingly important, following the recent introduction of coherent optical communications [2,3]. In addition, recent progress in synthesizing arbitrary optical waveforms [4–6] has intensified the effort toward providing simple and practical metrological methods to measure complex pulses having large time-bandwidth products (TBPs). These developments are creating a growing and compelling need for ultrafast coherent optical pulse measurement techniques that can operate at milliwatt peak power levels and on timescales ranging from sub-picoseconds to nanoseconds. Previous reports of ultrafast optical signal measurements in integrated, CMOS compatible platforms include time-lens temporal imaging and waveguide-based frequency-resolved optical gating (FROG) [1,7–10]. These approaches indeed transferred in the integrated domain two popular methods [1,11,12] for ultrafast pulse measurement; however, time-lens imaging is phase-insensitive while waveguide-based FROG methods require long integrated tunable delay lines - still an unsolved challenge for the full integration of the technique. Sheared interferometry, introduced by Walmsley [13] in 1998, is one of the most widely used methods for characterizing ultrafast optical pulses due to its ability to recover the full complex (i.e. amplitude and phase) information of an ultra-fast optical waveform. Most of its strength is due to a direct and robust algorithm [13–15] that retrieves the pulse from the spectra of two replicas of the same pulse, shifted (sheared) in frequency. The first and most popular implementation of sheared interferometry is named *spectral phase interferometry for direct electric-field reconstruction*, or SPIDER [1,13,14]. In the standard implementation of the SPIDER technique, the spectral shear between two replicas of the pulse under test (PUT) is obtained by nonlinearly mixing two delayed replicas of the PUT with a chirped pump pulse via a three wave mixing (TWM) process, as depicted

in Fig. 1. Each replica of the PUT must overlap with an almost monochromatic portion of the pump pulse in order to produce a nonlinear product with the same spectral shape of the PUT. As the two replicas mix with two different pump frequencies, the nonlinear product results in two pulses that are sheared in frequency. The pump pulse can be a dispersed replica of the PUT itself making this method remarkably self-referenced. In many cases, however, it is possible to use an external, well-characterized pump pulse, thus improving the accuracy of the method. In this case, the technique is usually referred to as cross-SPIDER or X-SPIDER [16,17]. In its many variants [1,13–20], SPIDER methods have proven to be well suited for the phase-sensitive characterization of ultra-fast laser pulses as short as 6fs, from the infrared to the ultraviolet.

Quite remarkably, the SPIDER method is fully compatible with designs that are amenable to waveguide implementation: recently [21], we reported a device capable of characterizing both the amplitude and phase of ultrafast optical pulses with the aid of a synchronized, incoherently related clock pulse. In this previous work, we revisited the X-SPIDER approach in order to exploit degenerate four-wave mixing (DFWM) interactions to allow its implementation in centro-symmetric materials. We demonstrated that the X-SPIDER can be implemented in CMOS compatible integrated platforms, offering a simple phase sensitive metrological device on a chip. To address the demand for efficient methods to monitor optical data streams with high TBP in optical networks, we introduced a novel extraction algorithm method, that we termed *FLEA*: *Fresnel-limited extraction algorithm*. The FLEA dramatically improves the accuracy of any X-SPIDER device (based both on 3rd order and more conventional 2nd order nonlinearities) for optical pulses having very large TBPs: thanks to this approach, we measured [21] pulses with a frequency bandwidth of >1 THz stretched up to 100 ps pulsewidths, yielding a TBP of >100.The FLEA removes a classical approximation in the X-SPIDER methods operating via nonlinear optical processes. In general, an X-SPIDER approach relies on the assumption of a pump pulse having a much larger chirp than the PUT.
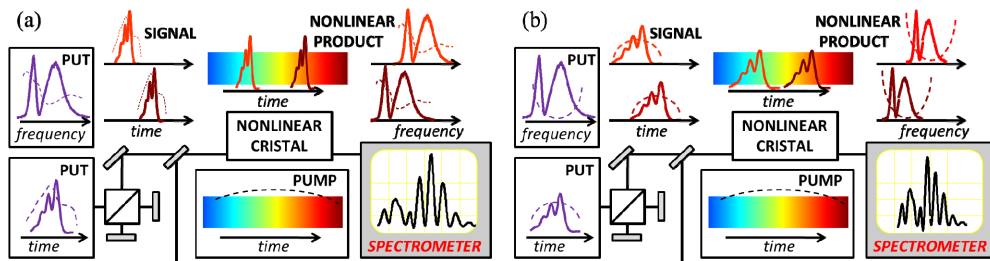

Fig. 1. (a) Sketch of the classical SPIDER setup for amplitude and phase retrieval. Two delayed replicas of the pulse under test (PUT) interact nonlinearly with a dispersed pump via frequency mixing in a bulk crystal. The nonlinear product is composed by two replicas shifted in frequency. Their spectrum is collected with a spectrometer and elaborated to extract the complete information (amplitude and phase) of the PUT. (b) Same interaction with a highly chirped PUT: in this case the two replicas of the signal cover a significant temporal portion of the pump and their spectrum is distorted when compared to the spectrum of the PUT. As a result, the standard algorithm fails to retrieve the PUT. Conversely, the FLEA is able to correctly work on this kind of pulses, by addressing the two replicas of the nonlinear product as a Fresnel Integral of the PUT.

If this condition is violated, the two replicas of the nonlinear product obtained by the wave mixing process depicted in Fig. 1 are no more spectral sheared replicas of the PUT. Hence, the information retrieved with the usual algorithm will exhibit a significant error. For this reason SPIDER methods are usually restricted to application on pulses with low TBP. Indeed, in most cases, significantly increasing the pump chirp is not an available option as it is accompanied by a reduction in the signal-to-noise ratio of the reconstructed profile. In general, sheared interferometry has been adapted for the measurement of highly chirped

pulses in several implementations. Pulses spanning from 400fs to 100 ps have been measured with a properly corrected electro-optical implementation of the sheared interferometry [22], while multiple shearing SPIDER algorithms are able to address pulses with large chirps and spectral holes or double pulses [23–26]. In any case, it is interesting to note that the nonlinear product of a standard SPIDER implementation always contains information on the phase of the PUT, and some retrieval strategies have been adopted for Gaussian pulses in the self-referenced case [20]. As detailed below, FLEA recognizes that the two replicas of the nonlinear product resulting in an X-SPIDER setup are a *Fresnel Integral* of the PUT, and implements the reconstruction process according to this observation, significantly extending the operating regime (TBP) of existing X-SPIDER setups.

In this paper, we present the full detailed theory of FLEA for X-SPIDER measurements, and include a detailed discussion of the inherent limits and tolerances of this phase-recovery approach. Our conclusions are validated through numerical examples on a standard test bench of pulses.

2. Parametric interaction and X-SPIDER

The PUT is represented in time and frequency by the temporal complex envelope of the electric field $e(t)$ and its spectrum $E(\omega)$, related to each other by the Fourier Transform:

$$e(t) = |e(t)| \exp\left[i\varphi_e(t)\right] = \int_{-\infty}^{\infty} E(\omega)\exp(-i\omega t)\frac{d\omega}{2\pi},$$

$$E(\omega) = |E(\omega)| \exp\left[i\varphi_E(\omega)\right] = \int_{-\infty}^{\infty} e(t)\exp(i\omega t)dt. \tag{2.1}$$

As is typically done, we restrict our analysis to bandwidth-limited pulses, i.e. where the PUT vanishes outside of the intervals given in time and frequency by $\Delta\tau_E$ and $\Delta\omega_E$, respectively. For both TWM and DFWM, the nonlinear interaction involves three optical waves: a pump $p(t)$ that amplifies a signal $s(t)$ and generates a nonlinear product ("idler" in DFG and DFWM cases) $i(t)$. As depicted in Fig. 1, the signal $s(t)$ consists of two delayed replicas of the PUT $e(t)$:

$$s(t) = \left[e\left(t + \frac{\Delta t}{2}\right) + e\left(t - \frac{\Delta t}{2}\right)\right] \tag{2.2}$$

The pump pulse is chirped in order to produce a temporal quadratic phase curvature with an envelope that is approximately constant over the duration span where nonlinear mixing with the signal occurs. Such a profile can be easily obtained by temporally stretching a transform limited pulse $p_o(t)$ with a flat-phase, smoothly varying spectrum $P_o(\omega)$, e.g. a spectrally bell-shaped or flat-top pulse over an interval $\Delta\omega_P$. After propagation through a predominantly first-order dispersive element with a total dispersion of $\phi_P = \beta_2 L$ (where L is the propagation length and β_2 is the group velocity dispersion of the dispersive element), the pump can be expressed in the frequency domain as

$$P(\omega) = P_o(\omega)\exp\left(-\frac{i\omega^2\phi_P}{2}\right) \tag{2.3a}$$

In the temporal domain, the pump is the *Fresnel Integral* of its transform-limited version $p_o(t)$:

$$p(t) = \frac{1}{\sqrt{2i\pi\phi_P}}\exp\left(\frac{it^2}{2\phi_P}\right) * p_o(t)$$

$$= \frac{1}{\sqrt{2i\pi\phi_P}}\exp\left(\frac{it^2}{2\phi_P}\right)\int_{-\infty}^{\infty} p_o(\tau)\exp\left(\frac{i\tau^2}{2\phi_P} - \frac{i\tau t}{\phi_P}\right)d\tau \tag{2.3b}$$

where the symbol * indicates the convolution operation. Under the assumption that $\phi_P(\Delta\omega_P)^2 >> 2\pi$, i.e. for a highly stretched pump, it is possible to use the Fraunhofer approximation of Eq. (2.3b):

$$p(t) \approx \frac{1}{\sqrt{2i\pi\phi_P}} \exp\left(\frac{it^2}{2\phi_P}\right) \int_{-\infty}^{\infty} p_o(\tau) \exp\left(-\frac{i\tau t}{\phi_P}\right) d\tau$$

$$= \frac{1}{\sqrt{2i\pi\phi_P}} \exp\left(\frac{it^2}{2\phi_P}\right) P_o\left(-\frac{t}{\phi_P}\right) \exp\left(\frac{it^2}{2\phi_P}\right)$$

$$(2.3c)$$

In this case the temporal amplitude of the stretched pulse follows the smoothly varying spectral shape $P_o(\omega)$, e.g. a bell shape or a nearly flat-top profile. The shape of the nonlinear product is dependent on the specific nonlinear process involved; in particular, considering valid the approximation (2.3c):

$$i(t) \propto s(t)p(t) \propto s(t)P_o\left(-\frac{t}{\phi_P}\right) \exp\left(\frac{it^2}{2\phi_P}\right) \approx s(t)\exp\left(\frac{it^2}{2\phi_P}\right) \qquad (2.4a)$$

$$i(t)^* \propto s(t)p(t)^* \propto s(t)P_o\left(-\frac{t}{\phi_P}\right) \exp\left(-\frac{it^2}{2\phi_P}\right) \approx s(t)\exp\left(-\frac{it^2}{2\phi_P}\right) \qquad (2.4b)$$

$$i(t)^* \propto s(t)\left[p(t)^*\right]^2 \propto s(t)\left[P_o\left(-\frac{t}{\phi_P}\right)\right]^2 \exp\left(-\frac{it^2}{\phi_P}\right) \approx s(t)\exp\left(-\frac{it^2}{\phi_P}\right) \quad (2.4c)$$

Equations (2.4a)–(2.4c) report the nonlinear product for the cases of TWM sum frequency generation (SFG), TWM difference frequency generation (DFG) and DFWM, respectively. The last approximations in the relations above are valid when the *pump temporal amplitude* or the *square of the pump temporal amplitude* for the TWM and DFWM cases respectively are almost constant along the temporal window $\Delta\tau_S$ occupied by the signal:

$$\Delta\tau_S = \Delta t + \Delta\tau_E \leq \Delta\tau_{PN} \qquad (2.5)$$

$\Delta\tau_{PN}$ is the temporal window defined by the pump in the nonlinear interaction and it is dependent on the specific shape taken into consideration. As outlined in Fig. 1, the nonlinear product is collected by a spectrometer, and so the experimental quantity of interest is the power spectral density (PSD) $|I(\omega)|^2$ of the nonlinear product, for the cases above:

$$|I(\omega)|^2 \propto |S(\omega) * P(\omega)|^2 \approx \left|S(\omega) * \exp\left(-\frac{i\omega^2\phi_P}{2}\right)\right|^2 \quad \text{TWM} - \text{SFG} \qquad (2.6a)$$

$$|I(\omega)|^2 \propto |S(\omega) * P^*(-\omega)|^2 \approx \left|S(\omega) * \exp\left(\frac{i\omega^2\phi_P}{2}\right)\right|^2 \quad \text{TWM} - \text{DFG} \qquad (2.6b)$$

$$|I(\omega)|^2 \propto |S(\omega) * P^*(-\omega) * P^*(-\omega)|^2 \approx \left|S(\omega) * \exp\left(\frac{i\omega^2\phi_P}{4}\right)\right|^2 \quad \text{DFWM} \qquad (2.6c)$$

For simplicity, in what follows, we will refer explicitly only to the case of SFG. As it is clear from the relations above, these results can be easily extended to the DFG case by simply changing the sign of the pump chirp, and to the DFWM case by changing the sign and dividing by 2 the pump chirp. Table 1 summarizes the results for Gaussian and flat top pulses

in the different nonlinear mixing cases. Focusing on the SFG case, it is useful to define

$$F_s(\omega) = S(\omega)\exp\left(-\frac{i\omega^2\phi_P}{2}\right) \qquad (2.7a)$$

The latter simply represents the output spectrum of the signal after an equivalent propagation in a first order dispersive system with the total dispersion of the pump ϕ_P, i.e. its Fourier Transform is the *Fresnel Integral* of the signal:

$$f_s(t) = \frac{1}{\sqrt{2i\pi\phi_P}}\exp\left(\frac{it^2}{2\phi_P}\right)\int_{-\infty}^{\infty}s(\tau)\exp\left(\frac{i\tau^2}{2\phi_P}-\frac{i\tau t}{\phi_P}\right)d\tau \qquad (2.7b)$$

With the above definitions, expanding the convolution operation, we recast Eq. (2.6a) as

$$\left|I(\omega)\right|^2 \propto \left|\exp\left(-\frac{i\omega^2\phi_P}{2}\right)\int_{-\infty}^{\infty}S(x)\exp\left(-\frac{ix^2\phi_P}{2}\right)\exp\left(ix\omega\phi_P\right)\frac{dx}{2\pi}\right|^2 =$$

$$= \left|\int_{-\infty}^{\infty}F_s(x)\exp\left(ix\omega\phi_P\right)\frac{dx}{2\pi}\right|^2 \propto \left|f_s\left(-\omega\phi_P\right)\right|^2 \qquad (2.8)$$

The nonlinear product is then proportional to the Fresnel Integral of the signal $f_s(t)$ defined in the equivalent temporal coordinate:

$$t_{eq} = -\omega\phi_P \qquad (2.9)$$

Considering the equivalent definitions for the Fresnel Integral of the PUT,

$$F_E(\omega) = E(\omega)\exp\left(-\frac{i\omega^2\phi_P}{2}\right) \qquad (2.10a)$$

$$f_e(t) = \frac{1}{\sqrt{2i\pi\phi_P}}\exp\left(\frac{it^2}{2\phi_P}\right)\int_{-\infty}^{\infty}e(\tau)\exp\left(\frac{i\tau^2}{2\phi_P}-\frac{i\tau t}{\phi_P}\right)d\tau \qquad (2.10b)$$

we have

$$\left|I(\omega)\right|^2 \propto \left|f_s\left(t_{eq}\right)\right|^2 = \left|f_e\left(t_{eq}+\frac{\Delta t}{2}\right)+f_e\left(t_{eq}-\frac{\Delta t}{2}\right)\right|^2 \qquad (2.11a)$$

This identity is the core of the FLEA algorithm, which relates the nonlinear product to the signal with the only constraints *on the pump pulse* being those given by Eq. (2.5). Equation (2.11a) contains the information on the phase $\varphi_{fe}(t_{eq})$ of $f_e(t_{eq})$, better seen by expressing Eq. (2.11a) as the sum of the three terms

$$\left|I(\omega)\right|^2 \propto dc\left(t_{eq}\right)+ac_+\left(t_{eq}\right)+ac_-\left(t_{eq}\right) \qquad (2.11b)$$

defined by the following relations:

$$dc\left(t_{eq}\right) = \left|f_e\left(t_{eq}+\frac{\Delta t}{2}\right)\right|^2 + \left|f_e\left(t_{eq}-\frac{\Delta t}{2}\right)\right|^2 \qquad (2.12a)$$

$$ac_\pm\left(t_{eq}\right) = \left|f_e\left(t_{eq}+\frac{\Delta t}{2}\right)\right|\left|f_e\left(t_{eq}-\frac{\Delta t}{2}\right)\right|\exp\left[\pm i\Delta\theta\left(t_{eq}\right)\right] \qquad (2.12b)$$

where $\Delta\theta(t_{eq})$ is the differential phase of the Fresnel Integral of the PUT:

$$\Delta\theta\left(t_{eq}\right) = \varphi_{fe}\left(t_{eq} + \frac{\Delta t}{2}\right) - \varphi_{fe}\left(t_{eq} - \frac{\Delta t}{2}\right) \qquad (2.12c)$$

Equation (2.12a) is the sum of the spectral moduli of the Fresnel Integral of the relatively delayed PUTs and does not contain any information on the phase of the PUT. We refer to this component as a "direct current" (DC) component as it is centered at zero in the equivalent frequency domain ω_{eq}. The phase information, Eq. (2.12c), is contained in Eq. (2.12b) and, as discussed later, its phase contribution typically results in a frequency displacement in the transformed domain. For this reason, we refer to these terms as "alternate current" (AC) terms. In a large number of cases the AC terms can be isolated from the DC components using a filtering procedure, and then transformed back to extract the differential phase, Eq. (2.12c). This is the very robust procedure introduced by Takeda, Ina and Kobayashy [15], generally employed in the classical SPIDER approach to extract the phase information of the optical field from the measured optical interferogram.

Table 1. Equivalent Quantities for the Nonlinear Interaction in Different Frequency Mixing Cases

	TWM (SFG)	TWM (DFG)	DFWM
Temporal window $\Delta\tau_{PN}$, Eq.(2.5)	Gaussian (waist): $\Delta\omega_P\phi_P$ Flat top (full width): $\Delta\omega_P\phi_P$	Gaussian (waist): $\Delta\omega_P\phi_P$ Flat top (full width): $\Delta\omega_P\phi_P$	Gaussian (waist): $\Delta\omega_P\phi_P /\sqrt{2}$ Flat top (full width): $\Delta\omega_P\phi_P$
Equivalent time, Eq. (2.9)	$t_{eq}=-\omega_P\phi_P$	$t_{eq}=\omega_P\phi_P$	$t_{eq}=-\omega_P\phi_P/2$
Effective chirp	ϕ_P	$-\phi_P$	$-\phi_P/2$

2.1 Convergence of high pump chirp approximation to the standard X-SPIDER formalism

Before presenting further details on the FLEA, we show that the standard relationships used in the X-SPIDER phase reconstruction process can be obtained from our more general expressions in Eqs. (2.11) and (2.12) by carrying out a Fraunhofer approximation of the Fresnel integral of the PUT, to explicitly obtain the shape of the PUT spectrum:

$$f_e(t_{eq}) \propto e\left(t_{eq}\right) * \exp\left(\frac{it_{eq}^2}{2\phi_P}\right) \approx E\left(-\frac{t_{eq}}{\phi_P}\right)\exp\left(\frac{it_{eq}^2}{2\phi_P}\right) \qquad (2.13a)$$

This approximation is strictly valid when

$$\Delta\tau_E^{\,2} << 2\pi\phi_P \approx 2\pi\frac{\Delta\tau_P}{\Delta\omega_P} \qquad (2.13b)$$

When the pump spectrum is larger or equal to the PUT spectrum, as it usually happens in X-SPIDER setups, Eq. (2.13b) necessarily implies that $\Delta\tau_E << \Delta\tau_P \approx \Delta\omega_P\phi_P$, i.e., the PUT temporal window must be much shorter than the pump time duration. The Fresnel Integral is thus proportional to the spectrum of the PUT. Substituting Eq. (2.13a) into Eq. (2.11a) and considering the definition of the temporal coordinate, Eq. (2.9), we derive the classical expression for the spectral-sheared interference pattern [1]:

$$|I(\omega)|^2 \propto \left| E\left(\omega + \frac{\Omega}{2}\right)\exp\left(+i\omega\frac{\Delta t}{2}\right) + E\left(\omega - \frac{\Omega}{2}\right)\exp\left(-i\omega\frac{\Delta t}{2}\right) \right|^2 \qquad (2.14a)$$

The pattern contains two spectral replicas of the PUT shifted in time and in frequency by Δt and Ω, respectively, the latter being the spectral shear defined as

$$\Omega = \frac{\Delta t}{\phi_P} \tag{2.14b}$$

The DC and AC components of Eq. (2.12) can be then written as

$$dc(\omega) = \left| E\left(\omega + \frac{\Omega}{2}\right) \right|^2 + \left| E\left(\omega - \frac{\Omega}{2}\right) \right|^2 \tag{2.15a}$$

and

$$ac_{\pm}(\omega) = \left| E\left(\omega + \frac{\Omega}{2}\right) \right| \left| E\left(\omega - \frac{\Omega}{2}\right) \right| \exp\left[\pm i\Delta\theta(\omega) \right] \tag{2.15b}$$

The latter is a measurable quantity that depends explicitly on the spectral differential phase of the PUT:

$$\Delta\theta(\omega) = \Delta\varphi_E(\omega) + \omega\Delta t = \varphi_E\left(\omega + \frac{\Omega}{2}\right) - \varphi_E\left(\omega - \frac{\Omega}{2}\right) + \omega\Delta t \tag{2.15c}$$

As anticipated, the derived equations are the classical expressions exploited by the standard SPIDER method, which directly targets the reconstruction of the spectral phase of the PUT.

3. Phase recovery algorithms

We next discuss how the FLEA works to reconstruct the PUT, by describing step by step the procedure in comparison with the classic approach. Similarly to the conventional phase-reconstruction SPIDER algorithm, FLEA requires a-priori knowledge on the time delay Δt and the effective chirp of the interaction ϕ_P.

3.1 Step 1: Takeda procedure for the extraction of the differential phase from the interferogram

The Takeda procedure [1, 13–15] can be in general applied to interferograms of different nature. The interferogram (2.11a) (or (2.14a) in its approximated form) can be described as the superposition of the "DC" and "AC" contributions in Eqs. (2.12a)-(2.12b). The AC contributions are responsible for the interference fringes and as a result, they can be extracted from the interferogram by applying a Fourier Transform procedure. Specifically, the Fourier Transform of the DC and AC components defined in Eqs. (2.12a)-(2.12c) in the space of ω_{eq} are

$$DC(\omega_{eq}) = \cos\left(\frac{\Delta t \omega_{eq}}{2}\right) \int_{-\infty}^{\infty} F_e\left(\frac{s + \omega_{eq}}{2}\right) F_e^*\left(\frac{s - \omega_{eq}}{2}\right) \frac{ds}{2\pi} \tag{3.1a}$$

and

$$AC_{\pm}(\omega_{eq}) = \frac{1}{2} \int_{-\infty}^{\infty} F_e\left(\frac{s + \omega_{eq}}{2}\right) F_e^*\left(\frac{s - \omega_{eq}}{2}\right) \exp\left(\mp \frac{is\Delta t}{2}\right) \frac{ds}{2\pi} \tag{3.1b}$$

Roughly speaking, if the fringes are very dense as compared with the PUT spectral bandwidth, the AC contributions will be well separated from the DC contribution in the transformed space, as sketched in Fig. 2. Since the AC components contain information on the spectral phase, one of them is filtered and then transformed back. The phase of the resulting signal is the differential spectral phase $\Delta\theta(t_{eq})$. It must be recalled that this operation cannot give any information on the *sign* of the differential phase, hence there is a degree of ambiguity. Rigorously the quantity obtained at this step is:

$$\mu\Delta\theta\left(t_{eq}\right) \tag{3.1.c}$$

Where μ can be ± 1 and is not known. In general, the issue of the separability of the terms in Eqs. (3.1a) and (3.1b) in the global Fourier Transform of the interferogram is nontrivial and depends on the unknown phase of the PUT. In Fig. 3 we report the DC and AC terms in the 2D phase space, i.e. as a function of the frequency ω_{eq} and of the delay Δt variables, for a Gaussian pulse with both first order and second order chirp. In the space $(\omega_{eq},\Delta t)$, we note that the AC terms have the shape of Wigner functions [1,27,28] - specifically, they are the cross-Wigner function of the Fresnel Integral of the PUT $f_e(t)$ and its time reversed copy $f_e(-t)$ in $(\omega_{eq},\Delta t)$ and $(\omega_{eq},-\Delta t)$, respectively. In these types of functions, a first order chirp generates a shear of the function along the straight line $\omega_{eq} = \Delta t/\phi$ where ϕ is the *total* first order chirp of the Fresnel integral of the PUT. For large values of ϕ the spectral content of the AC functions is nearly entirely localized along the loci $\omega_{eq} = \pm \Delta t/\phi$. In the same way the spectral content of the DC component shrinks around $\omega_{eq} = 0$: the integral term in Eq. (3.1.a) is simply the autocorrelation in the frequency domain of a signal centred in $\omega_{eq} = 0$, which typically shrinks when the first order dispersion increases.
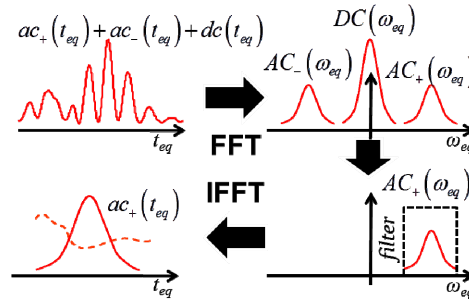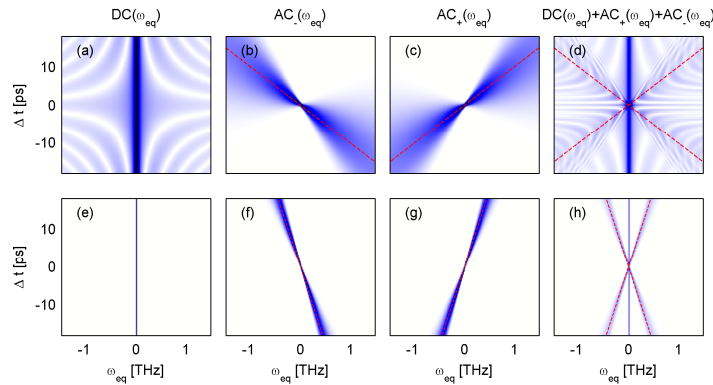

Fig. 2. Phase extraction procedure.

Fig. 3. (a) DC and (b-c) AC components as defined by Eqs. (3.1a)–(3.1b) in the phase space $(\omega_{eq},\Delta t)$, for a Gaussian PUT with first and second order chirps. The straight dashed line in red in (b-c) are the loci $\omega_{eq} = \pm \Delta t/\phi$, where ϕ is the *total* first order chirp of the Fresnel integral of the PUT, encompassing both the pump and the PUT chirps. In (d) the phase space representation of the complete interferogram is reported: in this case, the separation in frequency is not guaranteed for low values of the time delay Δt. (e-h) same as (a-d), but with a larger overall total dispersion ϕ: the spectral content of the DC (e) and AC (f-g) components is localized along $\omega_{eq} = 0$ and $\omega_{eq} = \pm \Delta t/\phi$, respectively. Thus, their separation in the interferogram (h) is guaranteed for a large set of delays Δt. Please notice that in (a), the pattern with hyperbolic loci around $\omega_{eq} \Delta t/2 = const$ is due to the cosine term $\cos(\omega_{eq}\Delta t/2)$ multiplying the integral in Eq. (3.1a). When the energy is localized for frequency components $|\omega_{eq}| < \pi/\Delta t$, as in the case (e) the hyperbolic pattern is not visible anymore.

This means that, roughly speaking, if the phase of $F_e(\omega_{eq})$ has a dominant first order chirp (as it *always* occurs in the classical SPIDER approximation, which is regulated by the pump chirp ϕ_P) encompassing both the pump and the PUT chirps, the spectral separation among the DC and AC terms is always ensured for a certain time delay Δt. Although the quantities are interpreted differently, Step 1 is the same as that conventionally used in the classical SPIDER reconstruction algorithm: the phase $\Delta\theta$ used in the classical algorithm is indeed the same quantity extracted here (i.e., function given by Eq. (2.12c)), but interpreted in its approximated form, Eq. (2.15c).

3.2 Step 2: extraction of the phase $\varphi_{fe}(t_{eq})$ from $\Delta\theta(t_{eq})$

The phase $\Delta\theta(t_{eq})$ must be processed to obtain the phase of the Fresnel Integral $f_e(t_{eq})$. It is important to note that although the phase extraction cannot provide the sign of $\Delta\theta$, this information can be recovered with the strategies described below. For a sufficiently small temporal delay Δt, the differential phase is the derivative of the phase $\varphi_{fe}(t_{eq})$:

$$\mu\Delta\theta\left(t_{eq}\right) = \mu\left(\varphi_{fe}\left(t_{eq}+\frac{\Delta t}{2}\right)-\varphi_{fe}\left(t_{eq}-\frac{\Delta t}{2}\right)\right) \approx \mu\frac{d\varphi_{fe}\left(t_{eq}\right)}{dt_{eq}}\Delta t \qquad (3.2)$$

We can directly integrate the result of Step 1 using the novel temporal coordinates introduced in Eq. (2.9):

$$\mu\int\Delta\theta\left(t_{eq}\right)\frac{dt_{eq}}{\Delta t} = -\mu\int\Delta\theta(\omega)\frac{\phi_P d\omega}{\Delta t} \approx \mu\varphi_{fe}\left(t_{eq}\right) \qquad (3.3)$$

In the last equality we took into account the physical quantities. It is interesting to note that even in this Step 2, FLEA follows closely the standard extraction procedure. If the approximated relation for the differential phase, Eq. (2.15c), holds, taking into account Eq. (2.14b), we have

$$-\mu\int\Delta\theta(\omega)\frac{\phi_P d\omega}{\Delta t} = -\mu\int\Delta\varphi_E(\omega)-\omega\Delta t\frac{d\omega}{\Omega} \approx \mu\left(\varphi_E(\omega)-\frac{\omega^2\phi_P}{2}\right) \qquad (3.4)$$

Equation (3.4) directly relates the differential phase obtained from Step 1 with the spectral phase of the PUT $\varphi_E(\omega)$. The additional quadratic term can be easily removed, as the pump effective chirp is known (indeed, the linear term $\omega\Delta t/\Omega$ is usually removed before the integration). As the chirp of the pump is supposed dominant over the PUT phase for the classical SPIDER approximation, the ambiguity on the sign of $\Delta\theta$ is removed in this case.

For large spectral shears, the derivative approximation is no more valid and several effective approaches have been proposed to retrieve the phase of the spectral PUT. Among them, a very popular concatenation method reconstructs exactly the phase even for large spectral shears. This method is discussed in detail elsewhere [1,14], including discussions on the accuracy of higher order integration and concatenation based techniques for different pulse profiles [29,30]. It is beyond the scope of this paper to discuss in detail how these methods can improve the performances of the FLEA. However, as Step 2 follows exactly the standard reconstruction procedure, concatenation and higher order integration techniques can be equivalently employed also for the FLEA as done in the classical algorithm.

3.3 Step 3: reconstruction of the full function

The amplitude of a single replica of the nonlinear product is measured independently and associated with the reconstructed phase. In the standard SPIDER approach, this quantity represents the PUT spectrum: the measurement is then complete. The temporal profile can be obtained with a simple Fourier Transformation. It is important to note that the SPIDER method does not have any ambiguity in the sign of the temporal axis because the sign of the

phase is determined as discussed previously. If the spectrum of the PUT is known, it can be associated with the reconstructed phase for better accuracy.

In the case of the FLEA, the spectral measurement of a single replica of the nonlinear product associated to the reconstructed phase is interpreted as the Fresnel Integral of the PUT $f_e(t_{eq})$, which then needs to be inverted in order to obtain the PUT. As noted previously, the phase extraction procedure does not provide information on the sign of the phase. Strictly speaking, we have to take into account the two relations

$$\left| f_e\left(t_{eq}\right)\right| \exp\left(i\varphi_{f_e}\left(t_{eq}\right)\right) = f_e\left(t_{eq}\right) \tag{3.5a}$$

$$\left| f_e\left(t_{eq}\right)\right| \exp\left(-i\varphi_{f_e}\left(t_{eq}\right)\right) = f_e^*\left(t_{eq}\right) \tag{3.5b}$$

Equation (3.5a) is the correct Fresnel integral of the PUT, while Eq. (3.5b) is its conjugate copy, leading to a *wrong result*. To obtain the PUT we Fourier transform both of them. We then obtain the correct Fresnel Integral of the PUT in frequency (Eq. (3.6a)) as well as its conjugate and *frequency reversed* copy, Eq. (3.6b):

$$F_e\left(\omega_{eq}\right) = \left| E\left(\omega_{eq}\right)\right| \exp\left(i\varphi_E\left(\omega_{eq}\right) - i\frac{\phi_P \omega_{eq}^2}{2}\right) \tag{3.6a}$$

$$F_e^*\left(-\omega_{eq}\right) = \left| E\left(-\omega_{eq}\right)\right| \exp\left(-i\varphi_E\left(-\omega_{eq}\right) + i\frac{\phi_P \omega_{eq}^2}{2}\right) \tag{3.6b}$$

where we use Eq. (2.9a). To obtain the PUT we subtract the phase $\exp(-i\phi_P \omega_{eq}^2/2)$ and obtain the two results:

$$E\left(\omega_{eq}\right) = \left| E\left(\omega_{eq}\right)\right| \exp\left(i\varphi_E\left(\omega_{eq}\right)\right) \tag{3.7a}$$

$$E'\left(\omega_{eq}\right) = \left| E\left(-\omega_{eq}\right)\right| \exp\left(-i\varphi_E\left(\omega_{eq}\right) + i\phi_P \omega_{eq}^2\right) \tag{3.7b}$$

The Fourier Transform of the Fresnel Integral, Eq. (3.6a), has the same spectral amplitude as the PUT. If the spectrum of the PUT is not symmetric, Eqs. (3.6b) and (3.7b)—representing the incorrect result—can be easily recognized through a simple comparison with a spectral measurement of the PUT. Otherwise, for spectrally symmetric waveforms, additional information on the PUT is needed. A second measurement with a different pump chirp will get rid of this ambiguity; however, very often it is simply possible to infer the correct phase as the two results differ by a large phase term. As in the case of standard SPIDER, the correct result given by Eq. (3.7a) does not have any ambiguity in the time domain.

4. Numerical examples

Summarizing the preceding discussion, we can conclude that i) the FLEA removes the high chirp approximation for the pump pulse and ii) is nevertheless subject to the following main limitations:

· The time duration of the pump (under approximation Eq. (2.5)), which defines the temporal window of the interaction, must be known a priori.

· The applicability of the Takeda phase extraction procedure is somehow limited. It depends on the phase of the unknown PUT and is not known a priori, but becomes clear only once the measurement has been performed. In general, a larger pump chirp guarantees better performances.

· It is ambiguous in the sign of the phase for pulses with symmetric spectral amplitude. However this can be simply solved via an additional measurement.

To better quantify the limitations imposed by the first two points, and also to compare with the standard extraction procedure, we calculate the accuracy of FLEA on benchmark test pulses [29,30]. Specifically, we consider a pulse with Gaussian spectral amplitude:

$$E(\omega) = \exp\left(-\frac{\omega^2}{\Delta\omega_E^2}\right) \tag{4.1}$$

We use this spectrum with different spectral phase profiles, such as phase jumps, parabolic, cubic and quartic phases. This benchmark pulse has already been significantly discussed in connection with calculations of the accuracy and precision of SPIDER reconstruction techniques [29,30]. The pump pulse is assumed to possess a nearly flat-top spectral amplitude. Specifically, it is assumed to have a super-Gaussian shape and parabolic phase:

$$P(\omega) = \exp\left(-\frac{\omega^{16}}{\Delta\omega_P^{16}}\right)\exp\left(-\frac{i\omega^2\phi_P}{2}\right) \tag{4.2}$$

In the numerical tests we use pulses with frequency bandwidths of the order of those expected in ultrafast optical communications, i.e. $\Delta\omega_E = 2\pi'1\text{THz}$, $\Delta\omega_P = 2\pi'2\text{THz}$, and ϕ_P with values varying from 10ps^2 - i.e. the pump covers a temporal window of approximately 250ps (full width) - to 20ps^2 - i.e. spanning a 500ps time window. We discuss the performance of the method for both the TWM (SFG) and DFWM cases. The simulations are performed using the exact relation $i(t)\propto s(t)p(t)$ in Eq. (2.4a) and $i(t)\propto s(t)[p(t)^*]^2$ in Eq. (2.4c). Provided that the idler in the DFWM case falls in a frequency range well distinct from the pump frequencies, the absolute pump and signal frequencies are irrelevant for the following discussion. As discussed above, since we employ an almost flat-top pump, the effective temporal window in the two cases is the same when the pump is identical, while the effective chirp is opposite and half of the pump chirp for the DFWM case. We used 2^{16} samples with a temporal resolution of 40fs. To simulate proper experimental conditions, we also took into account the limited bandwidth of the spectrometer, which we set to 1GHz. This translates to an equivalent temporal window of 600ps for the measured signals. The temporal limitation due to the spectrometer is then weaker than the temporal restriction due to the pump used in these simulations. To quantify the accuracy, we evaluated the RMS error ε of the reconstructed PUT $E_R(\omega)$, compared with the original waveform $E(\omega)$:

$$\varepsilon = \left[\frac{\int_{-\infty}^{\infty}|E_R(\omega) - E(\omega)|^2 \frac{d\omega}{2\pi}}{\int_{-\infty}^{\infty}|E(\omega)|^2 \frac{d\omega}{2\pi}}\right]^{1/2} \tag{4.3}$$

Usually, RMS values below 0.02 are considered to be excellent reconstructions, while values above 0.2 are considered to fail the reconstruction [29,30]. The delay between the two PUT replicas is set to 6.5 ps, and is chosen to minimize the error introduced by the integration of the differential phase, while allowing the filtering procedure for the standard algorithm. It is important to notice that larger delays can be used when applying concatenation of higher order integration procedure for the reconstruction of the differential phase also in the FLEA case.

4.1 Phase-jump pulses

We next apply phase jumps given by:

$$\varphi_E(\omega) = \frac{\pi}{2} \tan h\left(\alpha \frac{\omega}{\Delta\omega_E}\right) \qquad (4.4)$$

Where α is a parameter that indicates the steepness of the phase jump. Figure 4 shows the spectral amplitude (Fig. 4(a), black solid line) and phase for $\alpha = 10$ and $\alpha = 40$ (Fig. 4(b), black solid line and Fig. 4(d), dashed lines, respectively). In Fig. 4(a) and (b) we show the intensity of the nonlinear product replica generated by a SFG nonlinear interaction, for $\alpha = 10$ and $\alpha = 40$ (red solid and dashed lines, respectively).Here the pump possesses $\phi_P = 10ps^2$, $\Delta\tau_P =250ps$. This in turn translates into a significant distortion of the spectrum of the nonlinear product when compared with the original PUT spectrum. As discussed above, the distortion of the spectrum of the nonlinear product for the single replica is a clear indication that the high pump chirp approximation is exceeded. The phases reconstructed using both the classical algorithm and the FLEA are shown in Fig. 4, in red and green, respectively. (a-b) report the PSD for $\alpha = 10$ and $\alpha = 40$. The green plots indicate the PSD obtained with the FLEA reconstruction: remarkably the algorithm largely mitigates the distortion on the spectral amplitude visible in the replica of the nonlinear product - reported in red. The reconstructed phase is depicted in Fig. 4(c,d,e). For $\alpha=10$ both algorithms show good accuracy while for $\alpha=40$ the FLEA shows better performance, i.e. a lower RMS error, as discussed in Fig. 5.
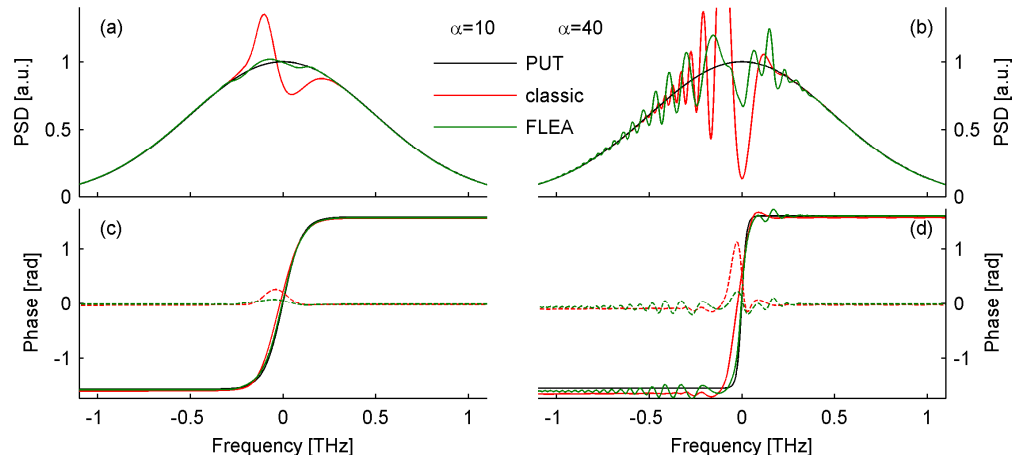

Fig. 4. Phase jump reconstruction. Here $\phi_P =10ps^2$, $\Delta\tau_P =250ps$. (a) PSD of the PUT (black) used in the simulation. The spectral amplitude for a single replica of the nonlinear product obtained with a PUT phase jump $\alpha=10$, and the PSD reconstructed with the FLEA are displayed in red and green lines, respectively. (b) same as (a) for a PUT phase jump $\alpha=40$. (c) PUT phase for $\alpha=10$, and reconstructed phases with the classical algorithm and FLEA in black, red and green solid lines, respectively. The dashed red and green lines report the differential error for classic algorithm and FLEA respectively. (d) same as (c) for $\alpha=40$.

In Fig. 5(a) and (b) the RMS error as a function of α is reported for both the standard algorithm (red) and the FLEA (green). Fig. 5(a) shows the error obtained with SFG. In Fig. 5(b) we used DFWM. We report in light red and light green the reconstruction obtained with a pump chirp $\phi_P = 10ps^2$ while dark red and dark green are used for the case of $\phi_P = 20ps^2$. In both cases, FLEA shows a significant reduction of the RMS error for high values of the phase jump parameter α, associated to longer temporal pulses. It is interesting to note that the RMS

error for the SFG case $\phi_P = 10\text{ps}^2$ follows closely the RMS error for the case DFWM $\phi_P = 20\text{ps}^2$. As we remarked above, the pump chirp counts half in the case of a DFMW interaction with respect to a TWM case. Hence, in the two cases the nonlinear interaction provides the same magnitude of equivalent chirp. Conversely, the DFWM interaction for $\phi_P = 20\text{ps}^2$ possesses an equivalent temporal window that is approximately twice the case of SFG with $\phi_P = 10\text{ps}^2$, and approximately equivalent to the case of SFG with $\phi_P = 20\text{ps}^2$. Indeed, the error is lower for larger pump chirps while it is insensitive to the dimension of the time window associated to the interaction, suggesting that the error for large α is not associated to the time window of the pump, but can be related instead to the increasing overlapping of the AC spectral components, Eq. (3.3b) for large α, which ultimately hampers the phase extraction procedure. In any case, the error remains remarkably low even for extremely steep phase jumps.
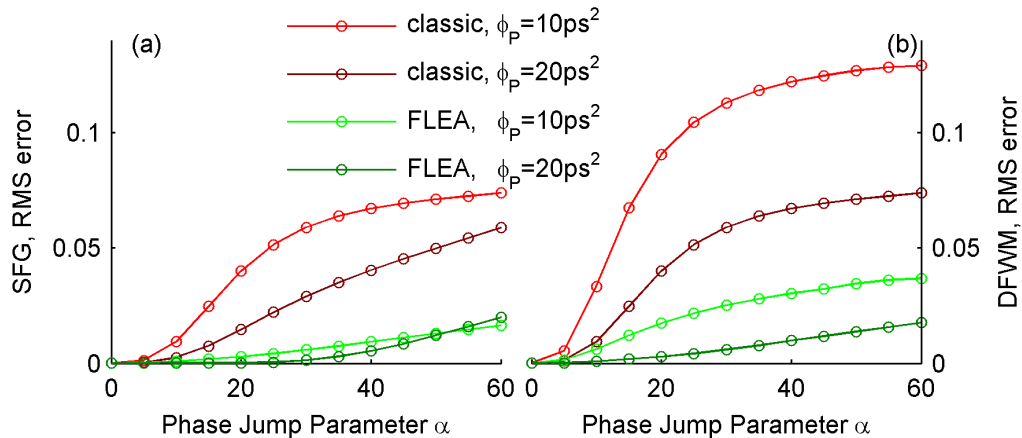

Fig. 5. RMS error as in Eq. (3) for the classic algorithm (red plots) and FLEA (green plots) vs α (higher values are for steeper phase jumps). (a) and (b) show the error calculated by using SFG and DFWM, respectively. Light red and light green are for $\phi_P = 10\text{ps}^2$, while dark red an dark green are for $\phi_P = 20\text{ps}^2$.

4.2 High order phase dispersion

Here we tested the performances of the FLEA applying first, second and third order dispersion to the PUT discussed above. The results in Fig. 6(a-d) are relative to first order dispersion phases for the classic algorithm and FLEA for a SFG (a-b) process and for the classic algorithm and FLEA for DFWM (c-d). They evidence a greatly extended range of consistency for the FLEA algorithm. The green dotted lines in (b) mark the maximum effective chirp that can be addressed due to the temporal limitation imposed by the pump temporal window. These lines are the same in the case of DFWM in (d). The cyan dotted lines in (b) report a "blind region" of the algorithm: for these values the chirp of the PUT exactly compensates the chirp of the pump. In this case the overall first order chirp of the Fresnel Integral is zero. As discussed in section 3.2, the fringes are not formed in the
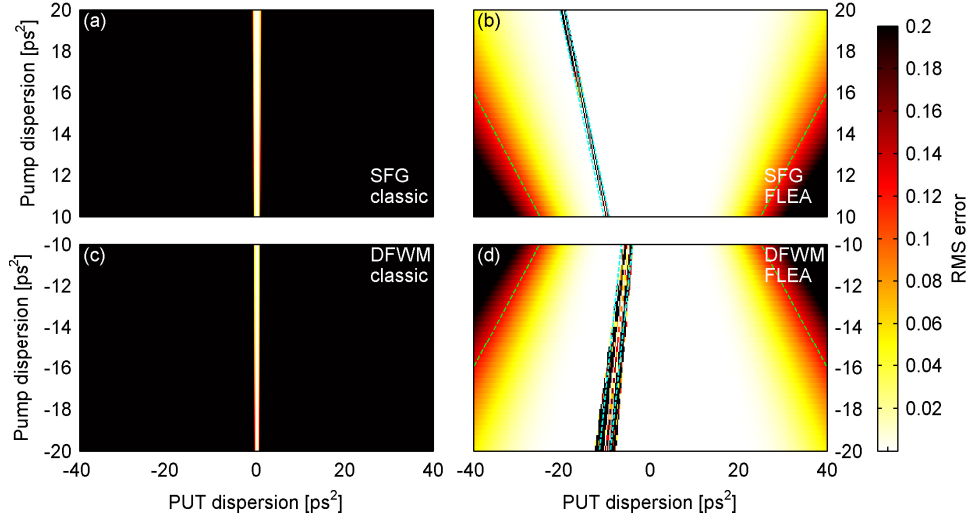
Fig. 6. Estimation of the accuracy of FLEA vs the standard algorithm for a PUT propagating through first order dispersive systems. (a,b) RMS error for the retrieved waveform vs pump (y axis) and PUT(x axis) total dispersions for the SFG case, and (c,d) for the DFWM case; (a,c) standard algorithm, (b,d) FLEA. The color bar reports the RMS error. The picture is saturated for RMS>0.2. In (b) the green dotted line corresponds to the limit imposed by the limitation of the pump temporal window and the cyan dotted lines report the "blind region" of the algorithm, around the opposite of the value of the pump dispersion. This graph clearly evidences that the low-error (white) zone is significantly increased when FLEA is used as compared to the standard algorithm. (c,d) same comments as (a,b) for the DFMW case.

interferogram and the Takeda Extraction procedure cannot be applied. The same region in (d) for the DFWM case is formed around the chirp values that compensate half of the pump chirp, with opposite sign. It is interesting to notice that the case of a Gaussian pulse with a first order chirp discussed here can be treated analytically, i.e. it is possible to find the correction of the chirp extracted by the Takeda procedure in a very similar fashion to what has been proposed for the SPIDER case in Ref. [20]; indeed, also using the exact correction of the extracted chirp the error follows the numerically calculated error as in Figs. 6(b) and 6(d).

Figure 7 shows the results for predominantly second order chirped pulses, with the same convention as of Fig. 6. The FLEA also extends the working regime of the X-SPIDER device in this case. The limitation for large second order chirps arises from the Takeda phase extraction procedure for the set of parameters exploited here, for pulses with both large positive and negative second order chirp, in a similar fashion to the example reported in Fig. 3. For this reason, the DFWM reconstruction for the FLEA shows a narrower range of consistency than the SFG case when the same pump is used, as the effective chirp of the nonlinear interaction is half of the pump chirp. However, in both cases the FLEA significantly extends the performance of the X-SPIDER setup. Figure 8 shows the results for predominantly third order chirped pulses. The limitations when large third order chirps are studied also arise from the Takeda phase extraction procedure for negative chirps, while the temporal window of the pump limits the reconstruction of the PUT with positive third order dispersions.
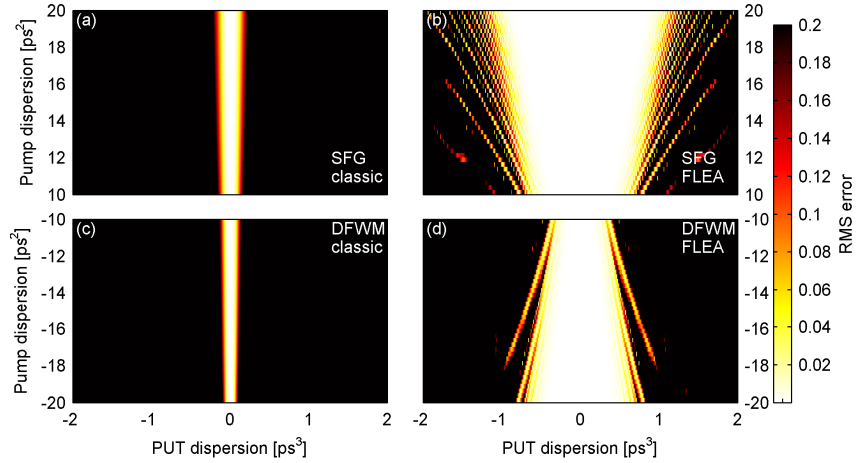
Fig. 7. Same as Fig. 6 for a PUT propagating through second order dispersive systems.
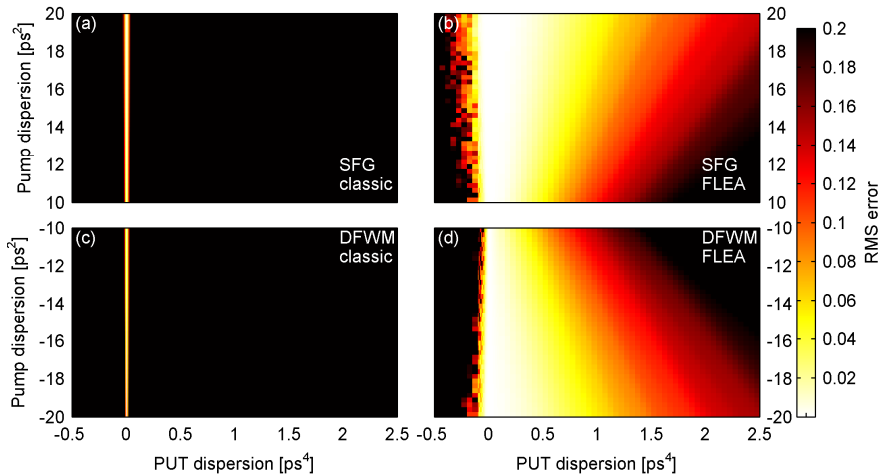

Fig. 8. Same as Fig. 7 for a PUT propagating through third order dispersive systems.

5. Conclusion

We have discussed the performances of an innovative extraction algorithm for X-SPIDER, that we term FLEA. We have discussed in detail the FLEA approach, and defined its limits for PUT reconstruction in terms of the physical parameters of the pump and the PUT. We evaluated numerically the performance of the FLEA, also in comparison with the standard X-SPIDER algorithm, for a conventional, comprehensive set of bench pulses: in all the addressed cases FLEA demonstrates a remarkably larger range of consistency in the reconstruction, evidencing a significant improvement in terms of time-bandwidth product of the reconstructed pulses.

Acknowledgments